# Site Specificity of Agonist-Induced Opening and Desensitization of the *Torpedo californica* Nicotinic Acetylcholine Receptor†

Iraida E. Andreeva,‡,§ Selvanayagam Nirthanan,|| Jonathan B. Cohen,|| and Steen E. Pedersen*,‡

*Department of Molecular Physiology and Biophysics, Baylor College of Medicine, Houston, Texas 77035, Bach Institute of Biochemistry, Russian Academy of Sciences, Moscow, Russia, and Department of Neurobiology, Harvard Medical School, Boston, Massachusetts 02115*

*Received August 11, 2005; Revised Manuscript Received October 26, 2005*

ABSTRACT: Agonist-binding kinetics to the nicotinic acetylcholine receptor (AChR) from *Torpedo californica* were measured using sequential-mixing stopped-flow fluorescence methods to determine the contribution of each individual site to agonist-induced opening and desensitization. Timed dansyl-C6-choline (DC6C) binding followed by its dissociation upon mixing with high, competing agonist concentrations revealed four kinetic components: an initial, fast fluorescence decay, followed by a transient increase, and then two characteristic decays that reflect dissociation from the desensitized agonist sites. The transient increase resulted from DC6C binding to the open-channel based on its prevention by proadifen, a noncompetitive antagonist. Further characterization of DC6C channel binding by the inhibition of [$^3$H]-phencyclidine binding and by equilibrium measurements of DC6C fluorescence yielded $K_D$ values of 2−4 $\mu$M for the desensitized AChR and ∼600 $\mu$M for the closed state. At this site, DC6C displayed a strongly blue-shifted emission spectrum, higher intrinsic fluorescence, and weaker energy transfer from tryptophans than when bound to either agonist site. The initial, fast fluorescence decay was assigned to DC6C dissociation from the $\alpha\delta$ site of the AChR in its closed conformation, on the basis of inhibition with the site-selective antagonists *d*-tubocurarine and α-conotoxin MI. Fast decay amplitude data indicated an apparent affinity of 0.9 $\mu$M for the closed-state $\alpha\delta$ site; the closed-state $\alpha\gamma$-site affinity is inferred to be near 100 $\mu$M. These values and the known affinities for the desensitized conformation show that the $\alpha\gamma$ site drives AChR desensitization to a ∼40-fold greater extent than the $\alpha\delta$ site, undergoes energetically larger conformational changes, and is the primary determinant of agonist potency.

The *Torpedo* nicotinic acetylcholine receptor (AChR)[1] is a ligand-gated ion channel with $\alpha_2\beta\gamma\delta$ stoichiometry and two distinct agonist-binding sites formed by $\alpha-\gamma$ and $\alpha-\delta$ subunit interfaces (*1*). Agonist binding to the two sites in the closed state induces a sequence of conformational transitions leading to channel opening followed by desensitization of the receptor (*2*). These transitions can be described as concerted allosteric changes that include large increases in agonist affinity (*3*, *4*) and changes in channel structure that affect permeability and affinity toward noncompetitive antagonists (*5*, *6*).

Desensitization has been further proposed to proceed through one or more intermediate conformations (*7*−*10*). Such conformations were initially invoked on the basis of transient affinities of binding for [$^3$H]ACh and for the fluorescent ACh analogue DC6C ($K_D$ values of 1−4 $\mu$M) that lie between the concentrations required to activate and those required to bind the fully desensitized state (*3*, *8*, *11*, *12*). An alternative nonconcerted model was proposed on the basis of binding studies of ACh, Carb, and epibatidine to embryonic mouse muscle receptor subunits expressed as intracellular $\alpha\gamma$ or $\alpha\delta$ dimers or as $\alpha_2\beta\gamma_2$ and $\alpha_2\beta\delta_2$ pentamers: desensitization at the first site occurs faster than subsequent desensitization at the second site, thereby constituting two phases of desensitization, fast and slow (*13*, *14*), without invoking a unique, intermediate agonist affinity. Recent electrophysiological studies of desensitization on adult mouse muscle AChR ($\alpha_2\beta\epsilon\delta$) have characterized up to five separate kinetic states (*15*).

The inherent asymmetry of agonist-site binding affinity likely contributes to the many components of desensitization. The antagonist *d*-tubocurarine binds with higher affinity to the $\alpha\gamma$ site of both AChRs (*1*), whereas the snail peptide toxin α-conotoxin MI binds with only slightly higher affinity to the $\alpha\gamma$ site of the *Torpedo* AChR and displays much higher affinity for the mouse muscle $\alpha\delta$ site than its $\alpha\gamma$ site (*16*−*18*). Epibatidine, a potent, large agonist, displayed site-selective binding to the $\alpha\gamma$ site (*19*, *20*). In contrast, the smaller agonist Carb bound to $\alpha\delta$ subunit pairs from mouse

† The work was supported in part by the R.A. Welch Foundation Grant Q-1406 (to S.E.P.), USPHS Grants NS35212 (to S.E.P.) and NS19522 (to J.B.C.), a Brooks Foundation Fellowship in Neurobiology (to S.N.), and a grant from Philip Morris USA and Philip Morris Intl. (to S.E.P.).

* To whom correspondence should be addressed. Telephone: (713) 798-3888. Fax: (713) 798-3475. E-mail: pedersen@bcm.tmc.edu.

‡ Baylor College of Medicine.

§ Bach Institute of Biochemistry.

|| Harvard Medical School.

[1] Abbreviations: ACh, acetylcholine; AChR, nicotinic acetylcholine receptor; α-BgTx, α-bungarotoxin; Carb, carbamylcholine; DC6C, dansyl-C6-choline; HTPS, HEPES-buffered *Torpedo* physiological saline; PCP, phencyclidine hydrochloride; TPS, phosphate-buffered *Torpedo* physiological saline.

10.1021/bi0516024 CCC: $33.50 
Published on Web 11/25/2005

muscle AChR with higher affinity than to $\alpha\gamma$ pairs (*21*), which could be largely attributed to four residues that differ between the $\gamma$ and $\delta$ subunits (*22*). However, only small affinity differences were observed for pentameric mouse AChRs in the desensitized state. Likewise, the *Torpedo* AChR in the desensitized state exhibited a small, 3-fold higher affinity for ACh and DC6C at the $\alpha\delta$ site (*11*). Electrophysiological studies indicate large, 100-fold differences in closed-state affinities of ACh for the *Torpedo* AChR sites (*23*), and similar, albeit smaller, differences were also observed for the embryonic mouse muscle receptor (*24*). The site-selective binding of small agonists, therefore, arises from differences in closed-state affinities rather than desensitized-state affinities. The data from the mouse muscle AChR point to the $\alpha\delta$ site as having higher closed-state affinity for the smaller agonists Carb and ACh, but this assignment is uncertain for *Torpedo* AChR.

DC6C has been extensively used as an agonist to characterize binding and conformational changes of the *Torpedo* AChR while largely assuming specificity of binding for the agonist sites. In previous work (*11*), we further showed that we could measure the extent of desensitization independently at each of the two binding sites from the amplitudes of the dissociation kinetics of bound DC6C. However, attempts to use sequential-mixing experiments to measure site-specific desensitization over the time course of agonist-induced opening and desensitization have been hindered by the complexity of the signals; in addition to the two distinct dissociations from the agonist sites, they also contain a fast decrease in fluorescence followed by a transient increase. Raines and Krishnan (*12*) initially proposed the fast decrease to reflect the release of DC6C from a closed-state agonist site with a $K_D \sim 1$ $\mu$M. The transient fluorescence increase was attributed to an open-channel block by DC6C in the presence of the high agonist concentrations that were used to induce dissociation of DC6C from the agonist sites.

To understand the detailed interactions of DC6C with the *Torpedo* AChR and the subsequent, induced conformational transitions, we characterized its interactions with the noncompetitive antagonist, channel site of the AChR, also called the agonist self-inhibitory site (*12*, *25*). Here, we show that DC6C binds the channel of the AChR in the open and desensitized states with a large shift in fluorescence emission wavelength. The optical and binding properties were used to specifically examine agonist-site binding in sequential-mixing stopped-flow experiments. Inhibition by site-selective antagonists revealed the fast, initial fluorescence decrease to result from dissociation of DC6C from the $\alpha\delta$ site. This result indicates that the $\alpha\delta$ site is the higher affinity site for the closed-state AChR and the lower closed-state affinity was assigned perforce to the $\alpha\gamma$ site. These assignments are incorporated into a model that is fully consistent with the equilibrium binding of DC6C and indicates that opening and desensitization are predominantly driven through the $\alpha\gamma$ site.

## MATERIALS AND METHODS

*Materials.* AChR-enriched membranes were obtained from *Torpedo californica* electric organ (Aquatic Research Consultants, San Pedro, CA) as described previously (*26*, *27*). Specific binding activity was measured by [$^3$H]ACh binding and is reported as ACh binding sites per milligram of protein. DC6C was synthesized according to Waksman et al. (*28*) as described (*29*). [$^3$H]PCP was obtained from Perkin−Elmer Life Sciences, Shelton, CT. [$^3$H]ACh (1.9 Ci/mmol) was kindly provided by Dr. Shaukat Husain (Massachusetts General Hospital, Boston, MA). Proadifen hydrochloride (SKF-522) was obtained from Research Biochemicals (Natick, MA). Carb chloride, decamethonium bromide, diisopropyl fluorophosphonate, hexamethonium chloride, (−)-nicotine hydrogen tartrate salt, PCP, and trimethylphenylammonium chloride were from Sigma−Aldrich (St. Louis, MO). *d*-tubocurarine was from ICN (Aurora, OH). α-Conotoxin MI was synthesized according to Papineni et al. (*16*). Other reagents were from standard sources.

*Fluorescence Measurements.* Fluorescence data were collected on an SLM 8000C fluorometer fitted with excitation and emission monochromators and a 450 W xenon short arc lamp light source. Emission spectra of DC6C binding to the AChR agonist binding sites and channel site were determined after a 1 h equilibration of AChR-rich membranes with DC6C and added ligands in *Torpedo* physiological saline buffer, HTPS (250 mM NaCl, 5 mM KCl, 3 mM $CaCl_2$, 2 mM $MgCl_2$, and 20 mM HEPES at pH 7.0). DC6C emission was monitored by changes in the fluorescence intensity under conditions of energy transfer from protein tryptophan(s) by excitation at $\lambda_{ex} = 282$ nm (*28*) or by direct DC6C excitation at $\lambda_{ex} = 340$ nm and filtered with a UV-pass filter (Oriel 59152), both at a 4.0 nm bandwidth. Emission was collected through a 390 nm cut-on filter (Oriel 51280).

Equilibrium DC6C binding to the noncompetitive antagonist site was measured by fluorescence enhancement by excitation at $\lambda_{ex} = 282$ nm with the UV-pass filter and emission collected at $\lambda_{em} = 467$ nm through a 430 nm cut-on filter (Oriel 51280). Data were collected in the presence or absence of 20 $\mu$M proadifen to determine background fluorescence, which was subtracted to determine specific fluorescence. Inhibition of DC6C binding to the noncompetitive antagonist site was measured by a fluorescence decrease at $\lambda_{em} = 467$ nm (4 nm bandwidth; 430 nm cut-on filter). Mixtures of DC6C, AChR-rich membranes, Carb, and various concentrations of proadifen or nicotine at pH 7.0 were equilibrated for 1 h prior to measuring fluorescence in a 10 × 10 mm quartz cuvette ($V = 1.03$ mL).

The kinetics of ethidium binding to the AChR noncompetitive antagonist site were measured by fluorescence enhancement on the SLM 8000C fluorometer, essentially as described previously (*30*). Concentrated ligand solutions were added to a 2 mL stirred AChR-rich membrane suspension in a 10 × 10 mm cuvette to yield the indicated final concentrations. Excitation was at $\lambda_{ex} = 322$ nm, filtered with a UV-pass filter; ethidium emission was collected at $\lambda_{em} = 605$ nm through a 550 nm cut-on filter (Oriel 59502).

*Fast Kinetic Measurements.* Experiments were carried out with a stopped-flow fluorescence instrument from KinTek Corporation (Model SF-2001, Austin, TX) with a 75 W xenon lamp light source. Fluorescence was excited at 285 nm selected by an excitation monochromator with a 4 nm slit width and a UV-pass filter (Oriel 59152). The emission signal was collected through a 495 nm cut-on filter (Oriel 51292), 460 nm (±40) nm band-pass filter (Oriel 57530), or 515 nm cut-on filter (Oriel 51294), as indicated. Single-mixing experiments to measure binding and dissociation

kinetics were carried out by mixing equal 30 $\mu$L volumes of two solutions. Individual shots (8−10) were averaged to reduce noise. Sequential-mixing experiments were carried out in the same instrument fitted with three syringes using a two-push protocol. The first push mixes the contents of two syringes and drives the mixture into a fixed-volume delay line (60 $\mu$L), typically mixing AChR with DC6C. The instrument pauses for a set delay time and then delivers a second push that forces the content of the delay line to mix with the content of the third syringe and pushes the final mixture into the fluorescence flow cell. Typically, the third syringe contains the blocking ligand in high concentrations: 3 mM Carb or 90 mM nicotine. The final concentrations in the cuvette are one-third the concentrations in the syringe, while the concentrations during the delay time are one-half the syringe concentrations.

*Radioligand-Binding Assays.* The equilibrium binding of [$^3$H]ACh and [$^3$H]PCP, in the presence of 1 mM Carb or 4 $\mu$M α-BgTx or absence of other ligands, to *Torpedo* AChR-rich membranes was determined as described (*31*). In brief, membrane suspensions, in TPS, *Torpedo* physiological saline buffered with 5 mM sodium phosphate at pH 7.0 were treated with diisopropylfluorophosphonate (∼0.5 mM) for 15 min to inhibit acetylcholinesterase activity, and radioligand binding was determined by centrifugation (15 000 rpm for 45 min) in a TOMY MXT-150 microcentrifuge. For [$^3$H]-ACh (80 nM), binding was measured using dilute membrane suspensions (1 mL assay volume, 80 mg of protein/mL, 40 nM ACh-binding sites), whereas for [$^3$H]PCP (6 nM), 200 $\mu$L aliquots of membrane suspensions at 0.7 mg of protein/mL were used. Membrane suspensions were equilibrated with [$^3$H]ACh for 30 min and with [$^3$H]PCP for 2 h, before centrifugation. Nonspecific binding was determined in the presence of 1 mM Carb for [$^3$H]ACh and in the presence of 1 mM proadifen (+Carb) or 1 mM tetracaine (−Carb) for [$^3$H]PCP. The averages of duplicate determinations were normalized to the binding determined in the absence of DC6C. The inhibition curves were fit to equations for single-site inhibition as described below.

*Data Analysis.* The experimental stopped-flow dissociation and binding rate data were fit to the following three-exponential function using the KinTek software:

$$F = A_1 e^{-k_1 t} + A_2 e^{-k_2 t} + A_3 e^{-k_1 t} + C \qquad (1)$$

where $F$ is the observed fluorescence intensity, $k_1$, $k_2$, and $k_3$ (also referred to as $k_{fast}$, $k_{\alpha\gamma}$, and $k_{\alpha\delta}$, respectively) are the rate constants for the dissociation or binding components, $A_1$, $A_2$, and $A_3$ are their respective fluorescence amplitudes, and $C$ represents the final level of observed fluorescence intensity. Fitting to two exponentials was to the same equation with $A_3 = 0$. In some cases, the data were first smoothed with a nine-point Gaussian filter.

Binding data were fit to the following single-site-binding equation:

$$F = AL/(K + L) + C \qquad (2)$$

where $F$ is the measured fluorescence, $A$ is the maximal fluorescence amplitude, $L$ represents the DC6C concentration, $K$ is the equilibrium binding constant, and $C$ represents the background fluorescence. Inhibition data were fit to the following single-site equation:

$$F = AIC_{50}/(IC_{50} + L) + C \qquad (3)$$

where $IC_{50}$ is the ligand concentration that produces 50% inhibition.

The bell-shaped plot of amplitudes for DC6C dissociation from desensitized αδ sites versus *d*-tubocurarine concentrations was fit to the empirical equation:

$$F = (A_0 + A_1/(1 + K/L))(1/(1 + L/IC_{50})) \qquad (4)$$

where $A_0$ and $A_1$ are the amplitudes for initial level of DC6C fluorescence (in the absence of *d*-tubocurarine) and the maximum increase, respectively, and $K_1$ and $IC_{50}$ are *d*-tubocurarine concentrations for 50% rise and fall in DC6C fluorescence amplitudes, respectively.

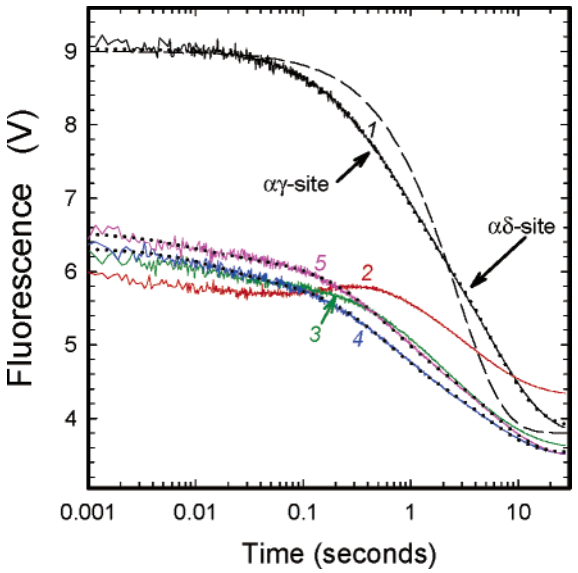


FIGURE 1: Proadifen and nicotine block DC6C binding to the AChR channel. The kinetics of DC6C dissociation from the AChR were measured by rapid-mixing with 60 mM nicotine using the single-mixing protocol described in the Materials and Methods (trace 1): AChR-rich membranes (0.15 $\mu$M ACh-binding sites) were pre-equilibrated with 1.5 $\mu$M DC6C in HTPS for 1 h prior to mixing. Nonequilibrium DC6C binding was measured using a sequential-mixing stopped-flow protocol (traces 2−5): AChR-rich membranes (0.3 $\mu$M ACh-binding sites) were mixed with 3 $\mu$M DC6C and held for 1 s in the delay line. DC6C dissociation was then recorded after mixing with 3 mM Carb, in the absence (2) or presence of 90 $\mu$M proadifen (3) or with 90 mM nicotine in the absence (4) or presence of 90 $\mu$M proadifen (5). Kinetic traces were recorded for 30 s and fit to two-exponential (curve 1, ⋯) or three-exponential (curves 4 and 5, ⋯) equations. For a comparison, a single-exponential fit to trace 1 is also shown (- - -).

## RESULTS

Rapid, low-affinity agonist binding to the AChR is followed by slower, induced conformational changes to a high-affinity, desensitized state. Equilibrium binding of the fluorescent agonist DC6C stabilizes the desensitized state, which has distinct affinities of 9 and 3 nM at the two nonequivalent αγ and αδ sites (*11*). DC6C dissociates from these two sites with characteristic, distinct rates, as illustrated by curve 1 in Figure 1. In this experiment, *Torpedo* AChR-rich membranes were equilibrated with DC6C and dissociation was then initiated by rapid mixing with excess nonflu-

orescent agonist in the stopped-flow instrument. The fluorescence was well-fit by a two-exponential decay corresponding to the loss of DC6C binding, with the faster component from the $\alpha\gamma$ site and the slower from the $\alpha\delta$ site (*11*); a single-exponential fit is shown by the dashed line for a comparison.

We wanted to use a sequential-mixing procedure to measure the kinetics of desensitization at each site by monitoring the decay amplitudes of high-affinity binding after various incubation times. The AChR would be rapidly mixed with DC6C, held in a delay tube for a predefined time to permit partial binding and desensitization, and then rapidly mixed with excess competing agonist to induce DC6C dissociation. However, with a short, 1 s time of DC6C binding and using excess Carb to initiate dissociation, sequential-mixing revealed two components in addition to the characteristic dissociations from the $\alpha\gamma$ and $\alpha\delta$ sites: a rapid decay with a time constant near 0.01 s and a transient enhancement with a time constant near 0.2 s (curve 2 in Figure 1). As characterized by Raines and Krishnan (*12*), the rapid decay corresponds to DC6C dissociation from a closed-state agonist site. The transient increase likely reflects an open-channel block by DC6C because of transient AChR activation upon mixing with Carb; channel binding may also account for the higher background fluorescence observed at the end of the trace.

Inclusion of the noncompetitive antagonist proadifen together with the Carb during the dissociation (curve 3) blocked the transient fluorescence enhancement, and the trace decayed to the lower background level, results that are consistent with open-channel binding by DC6C. The transient increase occurred at rates of 4−25 $s^{-1}$ (also see ref *12*). Because these rates are close to the characteristic 1−2 $s^{-1}$ rate of dissociation from the desensitized $\alpha\gamma$ site (see ref *11*), they interfere with quantitation of high-affinity $\alpha\gamma$-site binding.

*Nicotine Prevents DC6C Open-Channel Binding.* To reliably quantify DC6C binding by sequential-mixing, we examined conditions for initiating dissociation while avoiding DC6C open-channel binding. Although proadifen was effective in blocking the transient increase at low DC6C concentrations, at higher concentrations, this block appeared incomplete. We examined several partial agonists for their ability to block DC6C binding to the agonist sites and to prevent open-channel binding by causing less opening. Hexamethonium, decamethonium (*32*), phenyltrimethylammonium, and nicotine were tested for their ability to inhibit open-channel binding by ethidium (*33*). Nicotine was the best of these and had also been shown to be an effective open-channel blocker itself (*34*).

We tested whether nicotine yielded results similar to other agonists when used as a displacing ligand. For fully equilibrated, desensitized $\alpha\gamma$ and $\alpha\delta$ sites of AChR (curve 1 in Figure 1), the amplitude ratio ($A_{\alpha\gamma}/A_{\alpha\delta} = 0.62 \pm 0.04$, mean ± SD, $n = 4$) and the dissociation rates ($k_{\alpha\gamma} = 1.65 \pm 0.34$ $s^{-1}$, $k_{\alpha\delta} = 0.18 \pm 0.01$ $s^{-1}$) agreed with published kinetic parameters (*11*). In sequential-mixing experiments with nicotine, the fluorescent decay (curve 4) fits to three exponentials that correspond to fast dissociation of DC6C from a site in the closed state ($k_{fast} = 62$ $s^{-1}$) and dissociation from desensitized agonist sites with rates of $k_{\alpha\gamma} = 1.99$ $s^{-1}$ ($1.7 \pm 0.35$ $s^{-1}$, $n = 12$) and $k_{\alpha\delta} = 0.204$ $s^{-1}$ ($0.19 \pm 0.03$ $s^{-1}$). Further addition of proadifen to the nicotine blocking solution (curve 5) affected neither the efficacy of the channel block nor DC6C dissociation from the agonist binding sites: $k_{fast} = 114$ $s^{-1}$, $k_{\alpha\gamma} = 1.92$ $s^{-1}$ ($1.73 \pm 0.19$ $s^{-1}$, $n = 7$), and $k_{\alpha\delta} = 0.18$ $s^{-1}$ ($0.19 \pm 0.02$ $s^{-1}$). This shows that nicotine was effective in preventing channel binding and permits quantitation of $\alpha\gamma$- and $\alpha\delta$-site binding.

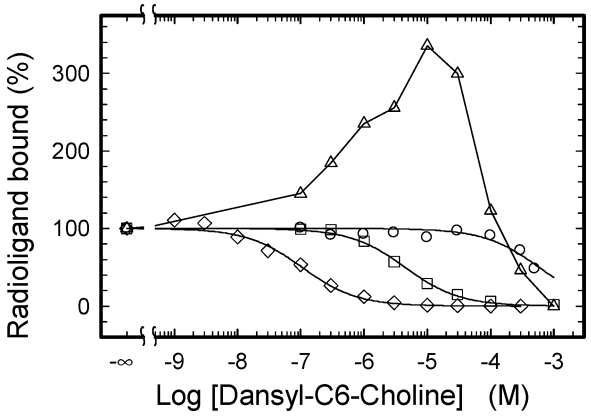


FIGURE 2: Equilibrium DC6C binding to the agonist and noncompetitive antagonist site. The effects of DC6C on the equilibrium binding of 80 nM [$^3$H]ACh to *Torpedo* AChR-rich membranes (◇) were determined as described in the Materials and Methods. The influence of DC6C on [$^3$H]PCP binding (6 nM) was determined in the absence of other ligands (△) or in the presence of 1 mM Carb (□) or 4 $\mu$M α-BgTx (○). The inhibition curves were fit to eq 3. For [$^3$H]ACh, $IC_{50} = 150 \pm 15$ nM. For [$^3$H]PCP in the presence of Carb, $IC_{50} = 3.9 \pm 0.3$ $\mu$M; in the presence of α-BgTx, $IC_{50} = 600 \pm 100$ $\mu$M. The binding of [$^3$H]PCP to nAChR-rich membranes in the absence of DC6C was 1440 ± 70 cpm (no added ligand), 4910 ± 90 cpm (+Carb), and 1544 ± 12 cpm (+α-BgTx). The binding of [$^3$H]ACh in the absence of DC6C was 25 500 ± 900 cpm. Nonspecific binding for [$^3$H]ACh was 720 ± 70 cpm and for [$^3$H]PCP, 575 ± 70 cpm (+Carb) and 620 ± 24 cpm (−Carb).

*Equilibrium DC6C Binding to the AChR Channel.* The ability of DC6C to bind the open channel of AChR suggests that DC6C may have the capacity to bind the channel site in other conformations of the AChR. As shown in Figure 2, DC6C displays biphasic effects on [$^3$H]PCP binding; low DC6C concentrations desensitized the AChR by binding the agonist sites and, thereby, enhanced affinity for PCP. Higher concentrations of DC6C inhibited PCP binding directly. In the presence of Carb, DC6C blocked [$^3$H]PCP binding with an $IC_{50}$ of 3.9 $\mu$M, while preincubation with α-BgTx resulted in inhibition at higher concentrations ($IC_{50} = 600$ $\mu$M). These results are consistent with DC6C binding to the AChR noncompetitive antagonist site preferentially in the desensitized conformation. We measured DC6C inhibition of [$^3$H]-ACh binding in parallel; the observed $IC_{50}$ value (150 nM) corresponds to a $K_D \sim 40$ nM after correction for the [$^3$H]-ACh concentration using the Cheng and Prusoff (*35*) method, a value that agrees with $K_D = 24-35$ nM that had been determined by fluorescence enhancement (*11*, *29*).

*DC6C Binding to the AChR Channel Results in Blue-Shifted Fluorescence.* Although the [$^3$H]PCP inhibition experiments demonstrated DC6C binding to the desensitized channel, preliminary experiments to measure associated fluorescence changes had detected little change at 550 nm, near the $\lambda_{max}$ for agonist-site binding. Accordingly, we analyzed the full emission spectra for DC6C bound at each site with excitation through tryptophan energy transfer ($\lambda_{ex}$

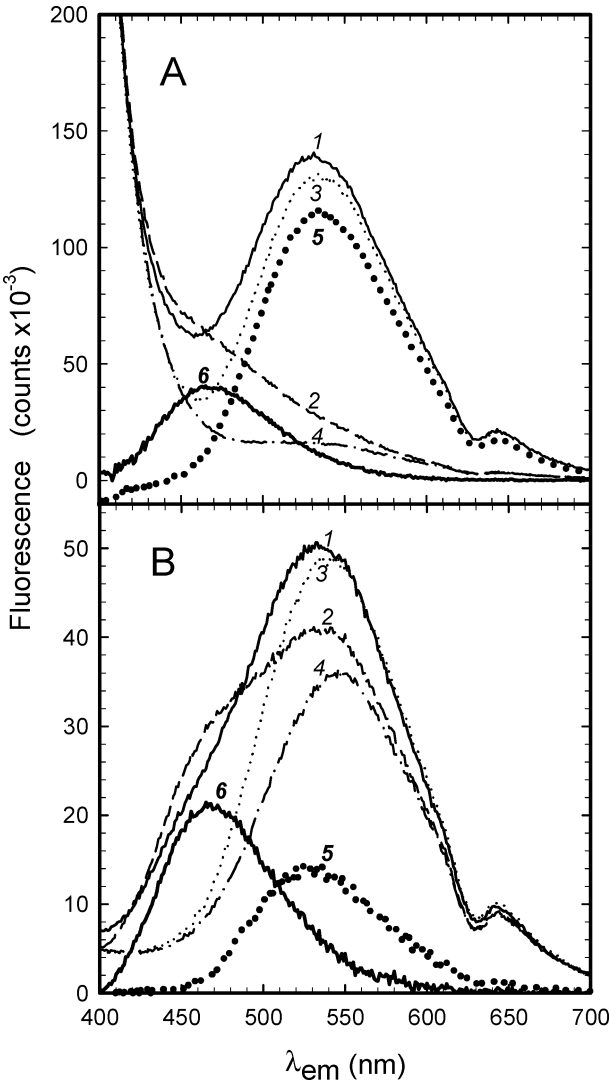


FIGURE 3: DC6C fluorescence is blue-shifted when bound to the noncompetitive antagonist site of the AChR. AChR-rich membranes (100 nM) in HTPS were incubated with 1 $\mu$M DC6C in the absence of additional ligands (1, —) or in the presence of 1 mM Carb (2, - - -), 30 $\mu$M proadifen (3, ···), or both (4, -·-). Difference spectra for agonist-site-bound DC6C (5, ···) are the difference between spectra 3 and 4 and, for the channel site (6, —), between spectra 2 and 4. The fluorescence emission spectra were recorded with excitation at 282 nm (A) and at 340 nm (B) as described in the Materials and Methods. The channel site difference spectra (spectra 6) have maxima at $\lambda_{max}$ = 465 nm; for the agonist sites (spectra 5), $\lambda_{max}$ = 535 nm.

= 282 nm, Figure 3A) and through direct excitation of the DC6C fluorophore ($\lambda_{ex}$ = 340 nm, Figure 3B). Spectra were taken in the absence of other ligands (spectra 1), in the presence of excess Carb (spectra 2), in the presence of proadifen (spectra 3), and in the presence of both ligands (spectra 4). In the absence of other ligands, excitation by tryptophan energy transfer showed a DC6C emission peak near 540 nm as well as tryptophan fluorescence near 400 nm (spectrum 1 in Figure 3A). Difference spectra were calculated for agonist-site-specific fluorescence (spectra 5 = 3 − 4) and channel-site-specific fluorescence (spectra 6 = 2 − 4). Channel-site fluorescence (spectrum 6) revealed a large 70 nm blue shift in the fluorescence maximum for DC6C relative to the agonist site (spectrum 5): $\lambda_{max}$ = 465 nm versus $\lambda_{max}$ = 535 nm. A similar shift was observed by direct excitation of the fluorophore (Figure 3B).

A comparison of the difference spectra showed a higher fluorescence yield from the channel site than from the agonist sites with direct excitation (compare spectra 6 and 5 in Figure 3B), even without accounting for the nearly full occupancy of the agonist sites and only 20−30% occupancy of the channel, on the basis of its binding constant. With tryptophan energy transfer, greater fluorescence is observed from the agonist sites (Figure 3A). To estimate the contribution of energy transfer to DC6C fluorescence, we obtained excitation difference spectra (data not shown) and compared the regions of tryptophan excitation (near 280 nm) with direct excitation of DC6C (near 340 nm). The difference spectra were further normalized to the excitation spectrum of free DC6C to correct for direct excitation of DC6C. While this method is imperfect, the calculated enhancement from energy transfer was greater at the agonist sites, 24.7 ± 0.2-fold, versus the channel site, 6.9 ± 0.2-fold, with emission measured at $\lambda_{em}$ = 560 nm; when emission was measured at $\lambda_{em}$ = 467 nm, the enhancements were 10.9 ± 0.1- and 3.73 ± 0.03-fold, respectively.

These data demonstrate that we can selectively monitor agonist-site binding versus channel binding by use of appropriate excitation and emission settings. To estimate the affinity of DC6C binding to the desensitized channel site by fluorescence enhancement, the AChR was titrated with increasing DC6C concentrations in the presence of Carb to block agonist-site binding and emission measured at 467 nm. A similar DC6C titration curve in the presence of proadifen served as a control (Figure 4A). The estimated $K_D$ value for DC6C binding to the desensitized channel corresponds to 2.1 ± 0.4 $\mu$M (inset in Figure 4A) and is in a good agreement with the $IC_{50}$ for DC6C inhibition of [$^3$H]PCP binding (Figure 2). Titration of bound DC6C with increasing concentrations of proadifen or nicotine, in the presence of Carb, was measured by the decrease in emission at $\lambda_{em}$ = 467 nm. The fitted $IC_{50}$ value for proadifen was 112 ± 30 nM (Figure 4B). Despite its apparently efficient open-channel block (*34*), nicotine required millimolar concentrations to block DC6C binding to the desensitized AChR channel ($IC_{50}$ = 18.3 ± 1.5 mM).

*Fast Kinetics of DC6C Binding to the AChR Channel Site.* Considering the substantial fluorescence signal of DC6C bound to the channel in steady-state measurements, it was important to determine whether such binding would affect the estimation of $\alpha\gamma$- and $\alpha\delta$-site dissociation. To compare directly the kinetics of DC6C binding to the channel site and agonist sites, we measured DC6C fluorescence changes during single-mixing experiments in the stopped-flow equipped with two photomultipliers. One had a 515 nm cut-on filter to pass predominantly emission from the agonist sites (Figure 5A), and the other had a 460 nm band-pass filter to monitor predominantly channel binding (Figure 5B).

Curve 1 in parts A and B of Figure 5 shows the kinetics of DC6C binding to the AChR after simple mixing in the absence of other ligands; the shape of the curve in Figure 5A is typical for our DC6C-binding experiments and could be fit to four exponentials (*11*). The shape of curve 1 in Figure 5B differs significantly, suggesting the presence of binding to the channel site as well. Curve 2 shows the results of mixing AChR with DC6C plus 1 mM Carb, which should evoke transient opening and open-channel binding by DC6C. The resulting fluorescence increase ($k$ = 5.3 ± 1.2 s$^{-1}$) was

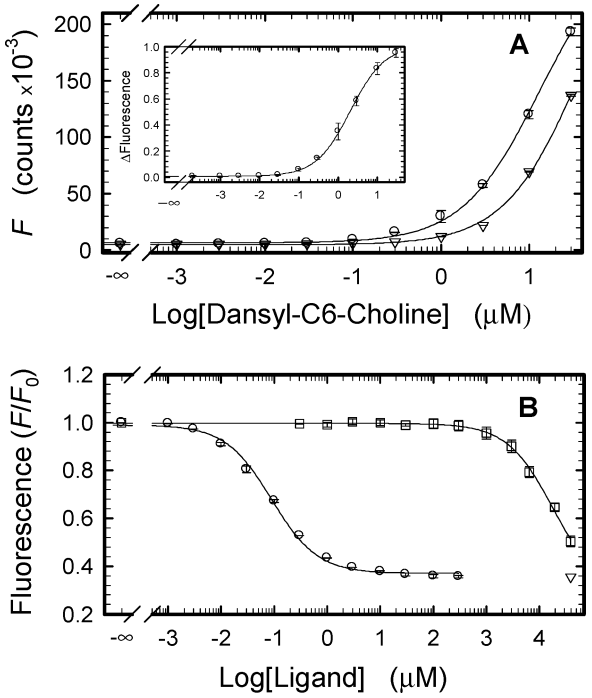


FIGURE 4: Noncompetitive DC6C binding to the desensitized AChR. (A) AChR-rich membranes (50 nM) were incubated for 40 min with 1 mM Carb and varying concentrations of DC6C in HTPS in the absence (○) or presence (▽) of 20 $\mu$M proadifen. DC6C fluorescence was determined as described in the Materials and Methods. Error bars represent the range of two independent determinations. (Inset) Specific binding data were normalized to the maximum value and plotted as the average and standard deviations of six independent determinations. The solid curve shows the best fit to the binding equation (eq 2) with $K_D = 2.0$ $\mu$M. (B) AChR-rich membranes (100 nM) in HTPS were incubated for 40 min with 1 $\mu$M DC6C, 1 mM Carb, and varying concentrations of nicotine (□), proadifen (○), or 20 $\mu$M proadifen plus 39 mM nicotine (▽). Fluorescence was determined as described in methods with $\lambda_{ex} = 285$ nm (or 292 nm in some experiments). For the nicotine titration, the data were corrected for fluorescence at high nicotine concentrations as determined in a parallel titration without DC6C. The data are plotted as the average and range of two independent determinations normalized to the control. The concentration dependence was fit to the equation for single-site inhibition (eq 3). The fitted $IC_{50}$ values are 18 mM for nicotine and 91 nM for proadifen.

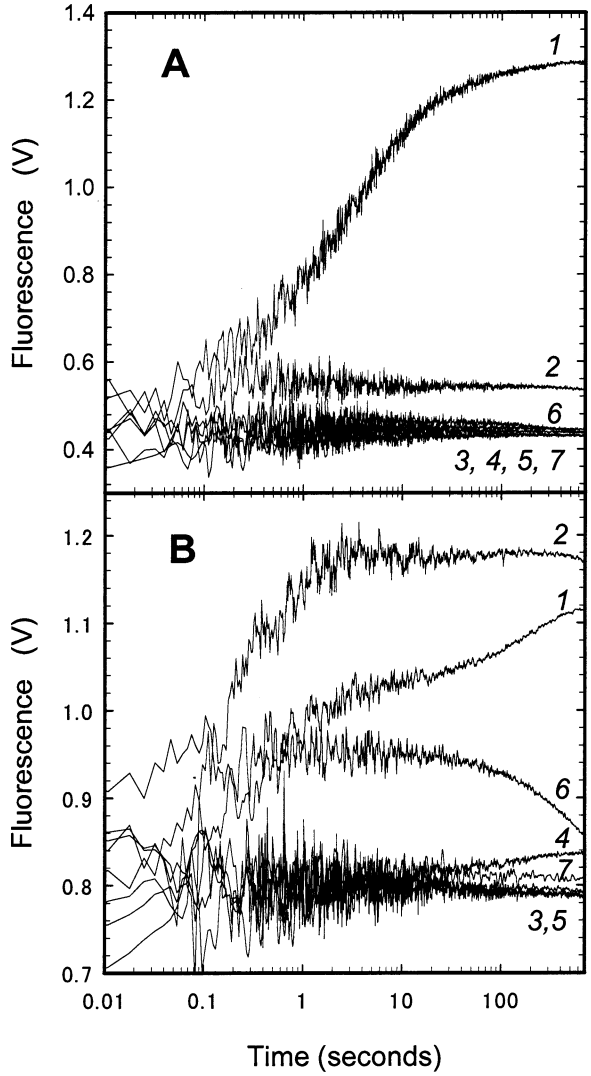


FIGURE 5: Fast kinetics of channel binding by DC6C. Kinetics of DC6C fluorescence were measured in stopped-flow single-mixing experiments using two photomultipliers with different filters for emission. (A) Data collected through a 515-nm cut-on filter. (B) Data collected through a 460-nm band-pass filter. The following pairs of solutions in HTPS were rapidly mixed using the single-mixing stopped-flow protocol described in the Materials and Methods: curve 1, AChR-rich membranes (0.4 $\mu$M) mixed with 4 $\mu$M DC6C; curve 2, AChR mixed with 4 $\mu$M DC6C and 2 mM Carb; curve 3, AChR mixed with 4 $\mu$M DC6C, 2 mM Carb, and 60 $\mu$M proadifen; curve 4, AChR and 1 mM Carb (pre-equilibrated for 1 h) mixed with 4 $\mu$M DC6C; curve 5, AChR and 1 mM Carb (pre-equilibrated for 1 h) mixed with 4 $\mu$M DC6C and 60 $\mu$M proadifen; curve 6, AChR, 1 mM Carb, and 2 $\mu$M DC6C (pre-equilibrated for 1 h) mixed with 2 $\mu$M DC6C plus 60 $\mu$M proadifen; curve 7, AChR and 2 $\mu$M α-BgTx mixed with 4 $\mu$M DC6C (2 $\mu$M AChR-rich membranes were pretreated for 2 h with 10 $\mu$M α-BgTx in 10 mM HEPES and then diluted to give HTPS).

greater when monitored at 460 nm (Figure 5B) and was blocked by proadifen (curve 3).

DC6C was mixed with AChR that had been pre-equilibrated with Carb to monitor the kinetics of DC6C binding to the desensitized receptor channel. Slow binding (curve 4) was detected with the 460 nm filter ($k_+ = 0.01 \pm 0.003$ s$^{-1}$) and was blocked by proadifen (curve 5), whereas only a small increase was detected above 515 nm. This association rate agrees with similar measurements made using a SLM 8000C fluorometer ($k_+ = 0.008 \pm 0.001$ s$^{-1}$). The rate was independent of the DC6C concentration in a range from 0.3 to 30 $\mu$M (data not shown). The dissociation rate from the channel was determined by pre-equilibrating the AChR with DC6C and Carb and then mixing with proadifen in the stopped flow (curve 6). The signal at 460 nm shows slow replacement of DC6C by proadifen ($k_- = 0.0019 \pm 0.0001$ s$^{-1}$); the dissociation was nearly indiscernible above 515 nm. Rapid mixing of α-BgTx-treated AChR with DC6C yielded no detectable increase in the fluorescent signal over the course of 20 min (curve 7).

*The αδ Site Has a Higher Agonist Affinity in the Closed State.* The rapid fluorescent decrease that occurred in the first 10 ms after sequential mixing (for example, see curve 2 in Figure 1) was assigned as the DC6C dissociation from a closed-state agonist site(s) by Raines and Krishnan (*12*). To distinguish whether this binding was predominantly to the αγ or αδ site, the AChR was prebound with increasing concentrations of site-selective competitive antagonists and the fast dissociation was analyzed by sequential-mixing stopped flow (Figure 6). Dissociation curves (see Figure 6A

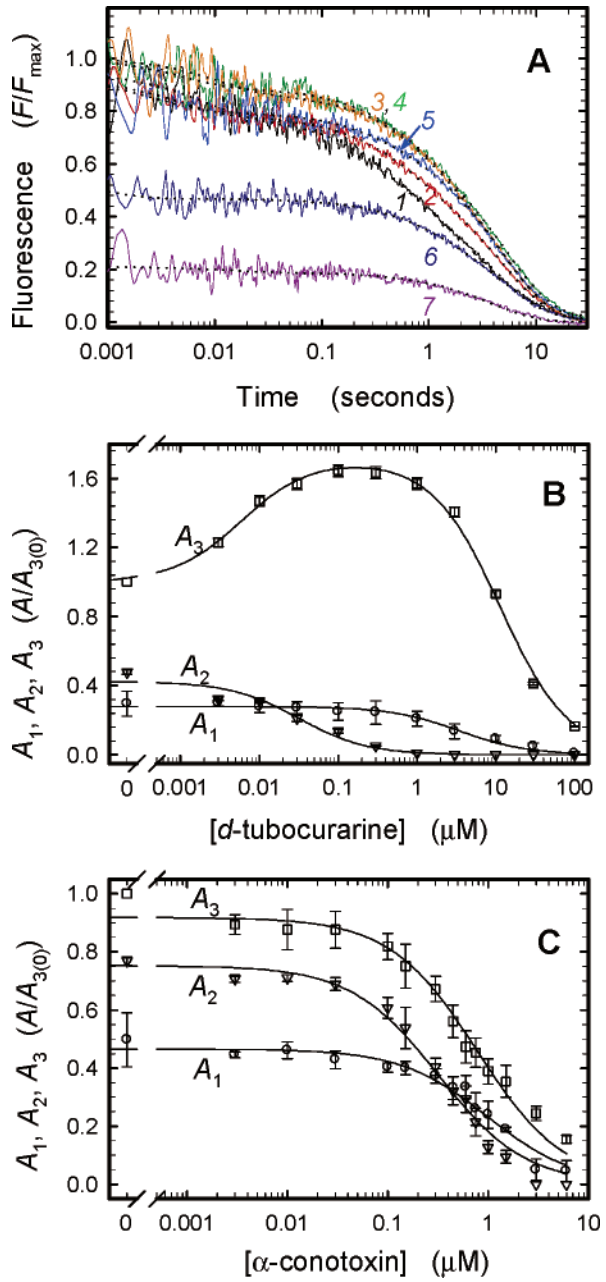


FIGURE 6: Rapid DC6C dissociation is from the αδ site in its low-affinity closed state. (A) AChR-rich membranes (0.12 $\mu$M) were preincubated in HTPS with various concentrations of *d*-tubocurarine (curve 1, 0 $\mu$M; curve 2, 0.003 $\mu$M; curve 3, 0.01 $\mu$M; curve 4, 0.1 $\mu$M; curve 5, 1 $\mu$M; curve 6, 10 $\mu$M; and curve 7, 30 $\mu$M). Sequential-mixing experiments were carried out by rapidly mixing the AChR−*d*-tubocurarine suspensions with 1.8 $\mu$M DC6C in the stopped-flow; DC6C dissociation was then induced after a 300 ms delay time by mixing with 3 mM Carb and 90 $\mu$M proadifen. Traces were recorded for 30 s, smoothed, normalized to the maximum signal, and fit to the three-exponential equation (···). (B) Amplitudes of DC6C dissociation corresponding to the fast ($A_1$) and slow ($A_2$ and $A_3$) decays were determined from the fits to traces, such as those in A, from AChR preblocked with various concentrations of *d*-tubocurarine. Amplitudes $A_1$, $A_2$, and $A_3$ were normalized to the $A_3$ value in the absence of *d*-tubocurarine. Each point is the average and range of two independent experiments. The data were fit to the inhibition equation (eq 3) or, for $A_3$, to eq 4. (C) Amplitudes of DC6C dissociation from AChR preblocked with different concentrations of α-conotoxin MI. The experiment was carried out as described for A and B with α-conotoxin MI as the competing ligand. Each point represents the average and standard deviation of three independent experiments.

for *d*-tubocurarine titration) were fit to three exponentials to determine the amplitudes of the fast dissociation ($A_1$), dissociation from the desensitized αγ site ($A_2$), and dissociation from the desensitized αδ site ($A_3$). The changes in these amplitudes at increasing *d*-tubocurarine concentrations are shown in Figure 6B. Inhibition of $A_2$ occurs with an $IC_{50} = 0.031 \pm 0.02$ $\mu$M, a value consistent with *d*-tubocurarine affinity for the αγ site. The dissociation amplitude from the desensitized αδ site, $A_3$, displayed biphasic behavior with increasing *d*-tubocurarine concentrations, with an increase at low concentrations and inhibition at higher concentrations. The increase can be attributed to *d*-tubocurarine binding at the αγ site with concomitant desensitization of the AChR, which then results in greater binding of DC6C to the αδ site (*11*). The $IC_{50}$ (13 ± 3.7 $\mu$M) for the inhibitory phase is consistent with *d*-tubocurarine affinity for the αδ site. The amplitude for the fast dissociation ($A_1$) was inhibited with an $IC_{50} = 3.93 \pm 1.92$ $\mu$M, which also corresponds to the affinity of *d*-tubocurarine to the αδ site (*1*).

A similar experiment was carried out with increasing concentrations of α-conotoxin MI (Figure 6C), which binds the *Torpedo* AChR αγ site with higher affinity and does not intrinsically induce desensitization. The fitted $IC_{50}$ values for inhibition of the three phases were as follows: $A_1$, $IC_{50} = 1.04 \pm 0.04$ $\mu$M; $A_2$, $IC_{50} = 0.36 \pm 0.04$ $\mu$M; and $A_3$, $IC_{50} = 0.83 \pm 0.04$ $\mu$M. The $IC_{50}$ for the $A_1$ phase most closely matches the $IC_{50}$ for $A_3$, which represents binding to the αδ site, suggesting that the $A_1$ phase represents αδ-site binding. This observation is consistent with the interpretation from the *d*-tubocurarine inhibition data. The rapid DC6C dissociation in sequential-mixing stopped-flow experiments, therefore, represents transient, low-affinity binding to the αδ site with a characteristic $k_{fast} = 100 \pm 30$ $s^{-1}$.

*The αγ Site Regulates Desensitization.* In their landmark description of the sequential-mixing kinetics of DC6C binding, Raines and Krishnan (*12*) characterized the rapid, initial fluorescence decline as the dissociation from a closed-state site because this component appeared too rapidly to reflect fast desensitization or other, slower allosteric changes. Furthermore, the magnitude and DC6C concentration dependence were consistent with a ~1 $\mu$M affinity and agreed with its observed dissociation rate of 100−200 $s^{-1}$. Our observations for this component are essentially consistent with theirs and show a similar affinity of 0.9 $\mu$M, as judged by the amplitude of this component at various DC6C concentrations (data not shown). The data in Figure 6 further argue that the rapid component reflects dissociation from the αδ site and, therefore, that it is the higher affinity closed-state site. While the closed-state affinity for the αγ site is not known, the values for binding of DC6C are similar to those of ACh itself, which has been shown to have about 100-fold difference in affinity for the two sites (*4*). Thus, the αγ-site closed-state affinity can be estimated to be near 100 $\mu$M.

The current estimates of closed-state affinity can be combined with the desensitized state affinities from Song et al. (*11*) into a scheme for binding to each site along with a conformational change to the desensitized state (see Figure 7; $\mathbf{A}_\gamma$ and $\mathbf{A}_\delta$ represent agonist binding). By further assuming an allosteric equilibrium between unliganded closed (**R**, for resting) and desensitized (**D**) conformations of $M = [\mathbf{D}]/[\mathbf{R}] = 0.05$ (*29*), the allosteric constants can be computed for

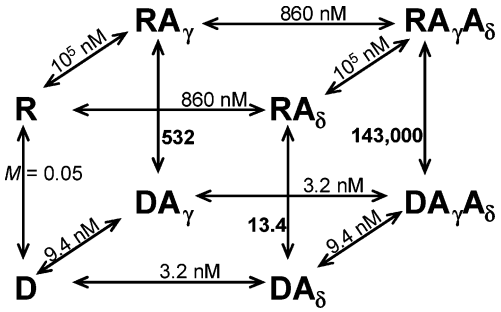


FIGURE 7: Allosteric model for desensitization of the AChR. See the text for a description.

each monoliganded equilibrium and for the diliganded equilibrium from thermodynamic cycle constraints (see the bold values in Figure 7). These values show that the $\alpha\gamma$ site undergoes a ~40-fold greater affinity change upon binding and consequently contributes 40-fold more to the net-ligand-induced desensitization of the AChR. Equilibrium DC6C binding according to this model was simulated using the kinetic modeling program VisKin (Zhang and Pedersen, unpublished results; the software can be downloaded at http://www.bcm.edu/physio/lab_pages/pedersen/index.html). The simulated data could be fit to the Hill equation with a $K_D$ = 24 nM and Hill coefficient $n$ = 1.53. These values agree reasonably well with the observed $K_D$ = 23 nM and $n$ = 1.35 observed by Song et al. (*11*).

## DISCUSSION

Ligand binding regulates the conformational paths of AChR opening and desensitization, possibly through several distinct or intermediate states. Sequential-mixing stopped-flow has been a useful technique for elucidating the rates and ligand dependence of desensitization in the AChR (*12*, *36*). To understand conformational regulation at a level of individual binding sites, it was necessary to determine the multiexponential nature of the stopped-flow signal. As part of this characterization, the spectral properties of binding of DC6C to the noncompetitive antagonist site of the AChR were determined as well as the kinetics of association and dissociation. Specific measurements of binding to agonist sites on closed and desensitized AChRs determined that the $\alpha\delta$ site constitutes the higher affinity closed-state site and, therefore, the $\alpha\gamma$ site has the lower closed-state affinity near 100 $\mu$M. This value indicates that the $\alpha\gamma$ site determines the potency of ACh for channel opening because the $\alpha\delta$ site will be fully occupied at concentrations required to titrate the $\alpha\gamma$ site. Because the $\alpha\gamma$- and $\alpha\delta$-site affinities only differ 3-fold for the desensitized state, the $\alpha\gamma$ site drives desensitization to a substantially greater extent than the $\alpha\delta$ site.

*DC6C as a Noncompetitive Antagonist of the AChR.* Equilibrium binding showed that DC6C has ~150-fold greater affinity for the noncompetitive antagonist site of the AChR in the presence of the agonist than in the presence of $\alpha$-BgTx, which stabilizes the closed state of the AChR; this result demonstrates substantially higher affinity of DC6C for the pore in the desensitized state. Binding was apparently competitive with PCP and proadifen, consistent with DC6C binding to the canonical binding site for channel blockers. There was a substantial spectral shift of 70 nm from $\lambda_{em}$ = 535 nm for binding the agonist sites to $\lambda_{em}$ = 465 nm for binding the noncompetitive antagonist site. In addition, the dansyl moiety had a higher fluorescence yield when bound to the channel, as observed by direct excitation of the fluorophore at $\lambda_{ex}$ = 340 nm and by considering the relative occupancy of the sites. In principle, this could be due to either a change in the quantum yield or to a change in the absorbance of the fluorophore. While the excitation spectra showed a small shift in the excitation maximum (data not shown), it seems more likely that there was an increase in the quantum yield. In contrast, a semiquantitative estimate of the fluorescence enhancement caused by tryptophan energy transfer showed that this was substantially higher at the agonist sites (as much as a 25-fold increase in the signal) than at the noncompetitive site (as much as a 7-fold signal increase). This is consistent with the known presence of tryptophan residues at the agonist sites and with examination of the structure of the AChR (*37*) near the channel that shows tryptophans to be near the outer lipid headgroups and more distant from the channel axis and the noncompetitive antagonist site. A similar shift of the emission maximum, albeit smaller at 15 nm, was observed for the noncompetitive binding of the homologous compound dansyl-choline to the *Torpedo marmorata* AChR (*38*). The large emission maximum shift and increased quantum yield of DC6C is consistent with shielding from the solvent at a hydrophobic binding site (*39*), an observation also consistent with binding to the canonical noncompetitive antagonist site.

DC6C also displays the property of rapid binding to the open channel, while binding to the AChR after its predesensitization with a high agonist concentration slowed both association and dissociation kinetics. This property has been observed for a number of other noncompetitive antagonists (*40*). In this case, the kinetics of the open-channel block have a maximal rate near 34 $s^{-1}$ (*12*), whereas channel binding to the predesensitized AChR had a rate near 0.01 $s^{-1}$, a change of at least $10^3$. Currently, there is no detailed structural model for the conformational change at the level of the channel during desensitization. The recent structural determinations of the transmembrane domain (*37*, *41*) likely reflect the closed state of the AChR, although this is not known with certainty. Labeling with 3-(trifluoromethyl)-3-*m*-([$^{125}$I]iodophenyl) diazirine suggested an open, water-accessible cavity for the desensitized conformation, relative to the closed state (*6*). However, the fluorescence accessibility of ethidium suggests that it was strongly shielded from water when bound in the desensitized conformation (*42*); likewise, a spin-labeled phencyclidine analogue was shown to be in a low dielectric environment in the desensitized conformation (*43*). The dramatic decrease in kinetic rates of binding to the desensitized state further suggests a physical barrier to exit and entry to the channel that effectively traps the ligand in the binding site. Such a barrier may constitute a desensitization gate that lies between the binding site and the extracellular milieu. While it is not clear whether a gate at this level would also provide a barrier to small cations, it seems likely that a conformational change in the vestibule or near the extracellular end of the M2-transmembrane helix undergoes a significant structural change upon desensitization that prevents ligand ingress and egress.

It was necessary to determine conditions for preventing the transient fluorescent increase resulting from open-channel

binding by DC6C during the sequential-mixing experiment. As well as displacing DC6C from the agonist sites, nicotine effectively prevented open-channel binding by DC6C, presumably because of its weak efficacy as an agonist on the muscle-type AChR (*44*) or its action as an open-channel blocker (*34*) or both. In addition, channel binding of DC6C to the desensitized state is slow enough that it is not observed during the normal 30 s time course of DC6C dissociation from the agonist sites. The data of Figure 5 indicate that open-channel binding of DC6C occurs to some extent prior to the addition of competing agonist. This can now be readily monitored by taking advantage of the spectral shift associated with channel binding. Nonetheless, while we can optically and pharmacologically isolate our observations of DC6C binding to the agonist sites, it may also be necessary to consider the effect of the channel block on the kinetics of conformational transitions.

*The αγ Site Regulates Channel Opening and Desensitization*. Channel opening generally requires higher concentrations than the low micromolar ACh concentrations required to bind the closed-state αδ site (*3*, *23*), assuming the ∼1 μM affinity determined here. This value is consistent with the affinity of ∼1 μM determined for [$^3$H]ACh binding to the *Torpedo* AChR upon rapid mixing and filtration (*45*). The net potency of ACh for channel-opening depends primarily upon double occupancy of the AChR along with the forward and backward rate constants for channel opening. The αδ site will be fully occupied at lower concentrations, and the concentration dependence of channel opening is, therefore, governed largely by binding to the lower affinity αγ site. Similar agonist-site selectivity is observed for the embryonic mouse muscle AChR (*21*).

It has also been shown that the αδ site in the desensitized conformation has a somewhat higher affinity for DC6C and for ACh itself (*11*) than does the αγ site. While the αδ site is the higher affinity site in both closed and desensitized states, the difference in affinities between the αγ and αδ sites are larger in the closed state. Consequently, the αγ site undergoes an energetically more profound change upon desensitization than the αδ site, and binding to this site drives desensitization to the extent of 40-fold more than the αδ site.

Characterization of the binding properties of DC6C permitted us to determine the role of each site in regulating the nicotinic receptor. Finding that the αδ site constitutes the higher affinity site in the closed state, we can further conclude that the αγ site serves the primary role in defining the $EC_{50}$ of opening; it undergoes a larger affinity shift upon desensitization and contributes substantially more to the net energy of desensitization.

## ACKNOWLEDGMENT

We thank Nasrin Latif-Shooshtari and Inna Yanez-Orozco for their assistance in *Torpedo* membrane preparation and Dr. Robert Meltzer for his helpful discussion of the experiments.

## REFERENCES

1. Pedersen, S. E., and Cohen, J. B. (1990) *d*-Tubocurarine binding sites are located at α−γ and α−δ subunit interfaces of the nicotinic acetylcholine receptor, *Proc. Natl. Acad. Sci. U.S.A. 87*, 2785−2789.
2. Katz, B., and Thesleff, S. (1957) A Study of the "desensitization" produced by acetylcholine at the motor endplate, *J. Physiol. 138*, 63−80.
3. Neubig, R. R., and Cohen, J. B. (1980) Permeability control by cholinergic receptors in *Torpedo* postsynaptic membranes: Agonist dose−response relations measured at second and millisecond times, *Biochemistry 19*, 2770−2779.
4. Sine, S. M., Claudio, T., and Sigworth, F. J. (1990) Activation of *Torpedo* acetylcholine receptors expressed in mouse fibroblasts. Single channel current kinetics reveal distinct agonist binding affinities, *J. Gen. Phys. 96*, 395−437.
5. Boyd, N. D., and Cohen, J. B. (1984) Desensitization of membrane-bound *Torpedo* acetylcholine receptor by amine noncompetitive antagonists and aliphatic alcohols: Studies of [$^3$H]acetylcholine binding and 22$Na^+$ ion fluxes, *Biochemistry 23*, 4023−4033.
6. White, B. H., and Cohen, J. B. (1992) Agonist-induced changes in the structure of the acetylcholine receptor M2 regions revealed by photoincorporation of an uncharged nicotinic noncompetitive antagonist, *J. Biol. Chem. 267*, 15770−15783.
7. Edelstein, S. J., Schaad, O., Henry, E., Bertrand, D., and Changeux, J. P. (1996) A kinetic mechanism for nicotinic acetylcholine receptors based on multiple allosteric transitions, *Biol. Cybernetics 75*, 361−379.
8. Heidmann, T., Bernhardt, J., Neumann, E., and Changeux, J. P. (1983) Rapid kinetics of agonist binding and permeability response analyzed in parallel on acetylcholine receptor rich membranes from *Torpedo marmorata*, *Biochemistry 22*, 5452−5459.
9. Neubig, R. R., Boyd, N. D., and Cohen, J. B. (1982) Conformations of *Torpedo* acetylcholine receptor associated with ion transport and desensitization, *Biochemistry 21*, 3460−3467.
10. Steinbach, J. H., and Sine, S. M. (1987) Function of nicotinic acetylcholine receptors, *Soc. Gen. Physiol. Ser. 41*, 19−42.
11. Song, X. Z., Andreeva, I. E., and Pedersen, S. E. (2003) Site-selective agonist binding to the nicotinic acetylcholine receptor from *Torpedo californica*, *Biochemistry 42*, 4197−4207.
12. Raines, D. E., and Krishnan, N. S. (1998) Transient low-affinity agonist binding to *Torpedo* postsynaptic membranes resolved by using sequential mixing stopped-flow fluorescence spectroscopy, *Biochemistry 37*, 956−964.
13. Sine, S. M., and Claudio, T. (1991) γ- and δ-subunits regulate the affinity and the cooperativity of ligand binding to the acetylcholine receptor, *J. Biol. Chem. 266*, 19369−19377.
14. Prince, R. J., and Sine, S. M. (1999) Acetylcholine and epibatidine binding to muscle acetylcholine receptors distinguish between concerted and uncoupled models, *J. Biol. Chem. 274*, 19623−19629.
15. Elenes, S., and Auerbach, A. (2002) Desensitization of diliganded mouse muscle nicotinic acetylcholine receptor channels, *J. Physiol. 541*, 367−383.
16. Papineni, R. V., Sanchez, J. U., Baksi, K., Willcockson, I. U., and Pedersen, S. E. (2001) Site-specific charge interactions of α-conotoxin MI with the nicotinic acetylcholine receptor, *J. Biol. Chem. 276*, 23589−23598.
17. Sine, S. M., Kreienkamp, H. J., Bren, N., Maeda, R., and Taylor, P. (1995) Molecular dissection of subunit interfaces in the acetylcholine receptor: Identification of determinants of α-conotoxin M1 selectivity, *Neuron 15*, 205−211.
18. Hann, R. M., Pagan, O. R., and Eterovic, V. A. (1994) The α-conotoxins GI and MI distinguish between the nicotinic acetylcholine receptor agonist sites while SI does not, *Biochemistry 33*, 14058−14063.
19. Prince, R. J., and Sine, S. M. (1998) Epibatidine binds with unique site and state selectivity to muscle nicotinic acetylcholine receptors, *J. Biol. Chem. 273*, 7843−7849.
20. Milone, M., Wang, H. L., Ohno, K., Prince, R., Fukudome, T., Shen, X. M., Brengman, J. M., Griggs, R. C., Sine, S. M., and Engel, A. G. (1998) Mode switching kinetics produced by a naturally occurring mutation in the cytoplasmic loop of the human acetylcholine receptor epsilon subunit, *Neuron 20*, 575−588.
21. Blount, P., and Merlie, J. P. (1989) Molecular basis of the two nonequivalent ligand binding sites of the muscle nicotinic acetylcholine receptor, *Neuron 3*, 349−357.
22. Prince, R. J., and Sine, S. M. (1996) Molecular dissection of subunit interfaces in the acetylcholine receptor. Identification of residues that determine agonist selectivity, *J. Biol. Chem. 271*, 25770−25777.
23. Sine, S. M., Claudio, T., and Sigworth, F. J. (1990) Activation of *Torpedo* acetylcholine receptors expressed in mouse fibroblasts.

Single channel current kinetics reveal distinct agonist binding affinities, *J. Gen. Phys. 96*, 395−437.
24. Zhang, Y., Chen, J., and Auerbach, A. (1995) Activation of recombinant mouse acetylcholine receptors by acetylcholine, carbamylcholine, and tetramethylammonium, *J. Physiol. 486*, 189−206.
25. Raines, D. E., and Zachariah, V. T. (2000) Isoflurane increases the apparent agonist affinity of the nicotinic acetylcholine receptor by reducing the microscopic agonist dissociation constant, *Anesthesiology 92*, 775−785.
26. Pedersen, S. E., and Papineni, R. V. (1995) Interaction of *d*-tubocurarine analogs with the *Torpedo* nicotinic acetylcholine receptor. Methylation and stereoisomerization affect site-selective competitive binding and binding to the noncompetitive site, *J. Biol. Chem. 270*, 31141−31150.
27. Pedersen, S. E., Dreyer, E. B., and Cohen, J. B. (1986) Location of ligand-binding sites on the nicotinic acetylcholine receptor α-subunit, *J. Biol. Chem. 261*, 13735−13743.
28. Waksman, G., Fournie-Zaluski, M. C., and Roques, B. (1976) Synthesis of fluorescent acylcholines with agonistic properties: Pharmacological activity on Electrophorus electroplaque and interaction *in vitro* with *Torpedo* receptor-rich membrane fragments, *FEBS Lett. 67*, 335−342.
29. Song, X. Z., and Pedersen, S. E. (2000) Electrostatic interactions regulate desensitization of the nicotinic acetylcholine receptor, *Biophys. J. 78*, 1324−1334.
30. Lurtz, M. M., Hareland, M. L., and Pedersen, S. E. (1997) Quinacrine and ethidium bromide bind the same locus on the nicotinic acetylcholine receptor from *Torpedo californica*, *Biochemistry 36*, 2068−2075.
31. White, B. H., Howard, S., Cohen, S. G., and Cohen, J. B. (1991) The hydrophobic photoreagent 3-(trifluoromethyl)-3-*m*-([$^{125}$I]-iodophenyl) diazirine is a novel noncompetitive antagonist of the nicotinic acetylcholine receptor, *J. Biol. Chem. 266*, 21595−21607.
32. Liu, Y., and Dilger, J. P. (1993) Decamethonium is a partial agonist at the nicotinic acetylcholine receptor, *Synapse 13*, 57−62.
33. Rankin, S. E., Addona, G. H., Kloczewiak, M. A., Bugge, B., and Miller, K. W. (1997) The cholesterol dependence of activation and fast desensitization of the nicotinic acetylcholine receptor, *Biophys. J. 73*, 2446−2455.
34. Tonner, P. H., Wood, S. C., and Miller, K. W. (1992) Can nicotine self-inhibition account for its low efficacy at the nicotinic acetylcholine receptor from *Torpedo*? *Mol. Pharmacol. 42*, 890−897.
35. Cheng, Y., and Prusoff, W. H. (1973) Relationship between inhibition constant ($K_i$) and the concentration of inhibitor which causes 50% inhibition of an enzymatic reaction, *Biochem. Pharmacol. 22*, 3099−3108.
36. Raines, D. E., and Krishnan, N. S. (1998) Agonist binding and affinity state transitions in reconstituted nicotinic acetylcholine receptors revealed by single and sequential mixing stopped-flow fluorescence spectroscopies, *Biochim. Biophys. Acta 1374*, 83−93.
37. Unwin, N. (2005) Refined structure of the nicotinic acetylcholine receptor at 4 Å resolution, *J. Mol. Biol. 346*, 967−989.
38. Cohen, J. B., Weber, M., and Changeux, J. P. (1974) Effects of local anesthetics and calcium on the interaction of cholinergic ligands with the nicotinic receptor protein from *Torpedo marmorata*, *Mol. Pharmacol. 10*, 904−932.
39. Lakowicz, J. R. (1983) *Principles of Fluorescence Spectroscopy*, Plenum, New York.
40. Oswald, R. E. (1983) Binding of phencyclidine to the detergent solubilized acetylcholine receptor from *Torpedo marmorata*, *Life Sci. 32*, 1143−1149.
41. Miyazawa, A., Fujiyoshi, Y., and Unwin, N. (2003) Structure and gating mechanism of the acetylcholine receptor pore, *Nature 423*, 949−955.
42. Herz, J. M., and Atherton, S. J. (1992) Steric factors limit access to the noncompetitive inhibitor site of the nicotinic acetylcholine receptor. Fluorescence studies, *Biophys. J. 62*, 74−76.
43. Palma, A. L., and Wang, H. H. (1991) Molecular environment of the phencyclidine binding site in the nicotinic acetylcholine receptor membrane, *J. Membr. Biol. 122*, 143−153.
44. Akk, G., and Auerbach, A. (1999) Activation of muscle nicotinic acetylcholine receptor channels by nicotinic and muscarinic agonists, *Br. J. Pharmacol. 128*, 1467−1476.
45. Boyd, N. D., and Cohen, J. B. (1980) Kinetics of binding of [$^3$H]-acetylcholine to *Torpedo* postsynaptic membranes: Association and dissociation rate constants by rapid mixing and ultrafiltration, *Biochemistry 19*, 5353−5358.

BI0516024